ACADEMIC PRESS

Available online at www.sciencedirect.com

SCIENCE DIRECT®

Journal of Sound and Vibration 267 (2003) 1–28

JOURNAL OF SOUND AND VIBRATION

www.elsevier.com/locate/jsvi

Computational analysis for dynamic response of a rotating shaft on flexible support structure with clearances

K. Hu[a], Z.P. Mourelatos[b], N. Vlahopoulos[a,*]

[a] *Department of Naval Architecture and Marine Engineering, The University of Michigan, 2600 Draper Road, Ann Arbor, MI 48109-2145, USA*

[b] *Vehicle Analysis & Dynamics Lab, Research & Development Center, General Motors Corporation, 30500 Mound Road 106, Box 9055, Warren, MI 48090-9055, USA*

Received 2 February 2002; accepted 16 September 2002

Abstract

A finite element-based formulation for modelling the dynamic behavior of a rotating flexible shaft supported by a flexible support structure is presented. The coupling effect between the rigid-body rotation and the flexible deformation of the shaft is considered and represented by non-linear coupling terms in the mass matrix and forcing vectors in the global system of equations. The rigid-body rotation is treated as one of the degrees of freedom (d.o.f.) of the entire system. The interaction between the rotating shaft and the flexible support is modelled by either linear or non-linear springs distributed around the circumference of the shaft. The coupling between the flexibility of the shaft and the flexibility of the support structure are considered. The flexible d.o.f. of both the shaft and the support structure are represented as a set of retained and internal d.o.f. of a Craig–Bampton formulation. An additional transformation is performed when the rigid-body d.o.f. is coupled with the internal and the retained d.o.f. in a Craig–Bampton basis. The equations of motion are solved in the time domain using a modified Newmark method for time integration, in which the Newton–Raphson method is used for handling the non-linear behavior within each time step. Analyses are performed to validate the new development for different combinations of load condition, spring type, and rigid-body rotation.

1. Introduction

Coupling rigid- and flexible-body dynamics of rotating structures has been studied in the literature extensively. The interaction between a rotating shaft and its support has also been a

*Corresponding author. Tel.: +1-734-764-8341; fax: +1-734-936-8820.
E-mail address: nickvl@engin.umich.edu (N. Vlahopoulos).

0022-460X/03/$ - see front matter
doi:10.1016/S0022-460X(02)01392-5

widely discussed topic. However, the interaction between a rotating flexible shaft and a flexible support structure at a system level has been very seldom addressed in the literature. A review summary on related topics is presented first.

Several papers have been presented in the past for modelling the combined rigid- and flexible-body dynamics of beams. A theory that allows computing small vibrations of a general rotating beam subjected to prescribed base excitation was presented [1]. A varying cross-section and material properties were considered for the beam. The effects of centrifugal stiffening and of the vibration induced by Coriolis forces were included in the formulation. A radially rotating flexible beam fixed to a rigid body was analyzed [2]. A set of fully coupled non-linear equations of motion was derived using the extended Hamilton principle. The effect of the coupling terms between rigid-body and flexural motion on the vibration was investigated. It was identified that for small values of the ratio between the flexible rigidity and the rigid inertia of the beam, the uncoupled equations led to substantially incorrect results. A computational procedure for multi-body dynamics analysis based on a finite deformation beam model was presented [3]. The beam formulation was based on fully non-linear strain measures that remain invariant with respect to the rigid-body motions. An inertial reference system was used for the beam dynamics, and the flexible degrees of freedom (d.o.f.) were computed with respect to a convected reference frame that rotates with the beam components. The development was targeting computations of the dynamics of flexible beams that undergo a variety of structural deformations in addition to large overall motions. The free flexural vibrations of a spinning, finite Timoshenko beam for the six classical boundary conditions were solved analytically in Ref. [4]. Expressions for the mode shapes and the natural frequencies were derived. A flexible body dynamic formulation, called the augmented imbedded geometric approach, was developed for beam structures undergoing large overall motion in a two-dimensional space [5]. The elastic deformation was characterized as a superposition of a number of assumed global shape functions. Solutions for cantilevered or pinned–pinned beams were presented. A method of quadratic components was developed in Ref. [6] for analyzing rotating flexible structures using a system of non-linearly coupled deformation modes. The formulation utilizes a non-linear configuration space in which all the kinematic constraints are satisfied up to the second order. The effects of rotary inertia on the extensional tensile force and on the eigenvalues of beams rotating about the transverse axis were presented in Ref. [7]. A method for dynamic simulation of multi-body systems including large-scale finite element models of flexible bodies was presented in Ref. [8]. An optimal lumped inertia technique was developed in order to avoid computation of the coupling matrices between the rigid-body d.o.f. and the flexible d.o.f. in the finite element representation of the flexible bodies. Inertia was lumped optimally at a subset of nodes of the finite element model, thus, simplifying the evaluation of the coupling terms in the equations of motion. The equations of motion were derived using a non-linear formulation that retains second order terms in the strain–displacement relationship [9–11]. Thus, the effect of all the geometric elastic non-linearities on the bending displacement was accounted for, without the need to include the high-frequency axial modes of vibration [9]. A Lagrangian formulation was employed for deriving the dynamic equations for a rotating beam [10,11] where the flexible d.o.f. were expressed in terms of the analytically derived modal basis for a beam. The coupling terms between the rigid-body d.o.f. and the flexible d.o.f. were derived from the modal representation of the flexible d.o.f. A finite element formulation coupling the rigid- and flexible-body dynamics of a rotating beam was presented [12]. The flexible d.o.f. were represented

either as physical d.o.f. of beam elements or three-dimensional solid elements (no modal reduction) or as internal and retained d.o.f. of a Craig–Bampton formulation. The finite element shape functions of beam elements in a three-dimensional space and the shape functions of solid elements in a three-dimensional space were utilized to represent the flexible d.o.f. A new formulation for the coupling matrices and the coupling vectors was presented. In addition, when the Craig–Bampton formulation was used for reducing the physical d.o.f., a transformation was developed and imposed on the coupling matrices, in order to account for the relationship between the physical d.o.f. and the internal and retained d.o.f. of the Craig–Bampton formulation. The formulation presented in Ref. [12] is also employed in this paper for modelling the dynamic behavior of the rotating flexible shaft (Fig. 1).

An application area where a rotating shaft is supported by a flexible support structure through a non-linear connection can be identified in the field of crankshaft-block dynamics. In Ref. [13], a four-cylinder engine was analyzed. The Reynolds equation was solved for the lubrication film pressure and the bearing housing structure was approximated by distributed linear springs. The bearing housing surface was assumed locally rigid such that no local deflection occurs in the surface of the bearing housing. The rigid surface assumption simplifies the computation and the contribution to the clearance from the deformed bearing structure is neglected. A 'mobility method' for hydrodynamic analysis of the journal bearings with dynamic loads was presented in Ref. [14]. The journal center velocity was separated into the oil whirl and oil squeeze terms, while the dynamic problem was treated as a quasi-static initial-value problem. The mobility method was applied to the connecting-rod bearing and satisfactory results were obtained [15]. Although the mobility method is the simplest way to describe the oil film hydrodynamics, it neglects the important effects of the journal misalignment and its application is limited to short, full journal bearings with circumferential symmetry. A structural analysis using dynamic substructuring with Ritz vectors was presented for predicting the dynamic response of an engine crankshaft, based on the finite element method in Ref. [16]. It is common in crankshaft studies to represent the oil film hydrodynamics with either the mobility method [17–20] or simple spring–damper combinations [21–23]. In some cases the oil film is completely neglected [24] due to the complexity of coupling the lubrication analysis with the crankshaft structural analysis. The Reynolds equation was solved for the main bearing lubrication problems by finite element method [25,26]. A system model for analyzing the dynamic behavior of an internal combustion engine crankshaft was described in Ref. [25]. The model couples the crankshaft structural dynamics, main bearing hydrodynamic lubrication, and engine block stiffness. The static block stiffness was used neglecting therefore, the engine block mass inertia and dynamic behavior. Three linear springs were used along the bearing length to represent the engine block flexibility in both vertical and horizontal planes. The coupling

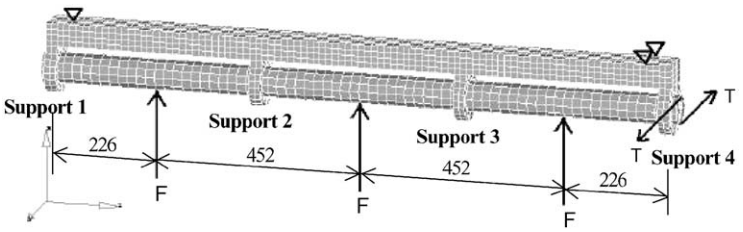

Fig. 1. A finite element model of rotating shaft and support structure.

between the vertical stiffness and the horizontal stiffness of the same bearing, as well as the coupling stiffness among different bearings, were neglected. Four d.o.f. (vertical and horizontal translations and rotations) are used for each bearing to account for the journal misalignment within the bearing [26]. The effects of oil grooves and oil holes of the bearing on the hydrodynamic behavior of the oil film were not considered. The Gumbel cavitation condition was used to save computation time at the cost of computational accuracy.

The work presented in this paper couples a detailed formulation for the rigid- and flexible-body dynamic behavior of a rotating shaft [12] with the dynamic behavior of a flexible support structure. The two structures are interconnected through non-linear springs distributed around the circumference of the shaft at every support location. The new developments presented in this work are as follows:

(1) Development of a specialized coupling algorithm between a flexible and rigid-body dynamic formulation of a rotating shaft with the flexible body dynamic equations of the support structure. The coupling algorithm is based on deriving a relationship between the interaction forces applied on the two components and the relative clearance between them. In the new coupling algorithm the flexible d.o.f. for both the shaft and the support structure are represented as a condensed set of internal and retained d.o.f. of a Craig–Bampton formulation. The new coupling algorithm incorporates a specialized transformation matrix between physical and Craig–Bampton d.o.f. at the support in order to properly capture the interaction between the two flexible members. The overall number of d.o.f. for the coupled system is significantly reduced compared to a physical representation of the flexible d.o.f.
(2) Development of the combined system of dynamic equations for the shaft and the support structure. The combined system of equations includes information about the rigid and flexible d.o.f. of the rotating shaft and the interaction between them. It also includes the flexibility of the supporting structure and the non-linear coupling between the shaft and the support, induced by the connecting non-linear springs. Both the coupling stiffness among different supports and the coupling stiffness between vertical and horizontal plane of the same support are included in this development.
(3) Development of a DMAP code within NASTRAN for evaluating the FEA-based matrices which are present in the combined system of dynamic equations.
(4) Application of the Newmark method modified by a Newton–Raphson iteration process within each time step for solving the combined non-linear system of dynamic equations.

2. Flexible dynamic response of support and shaft structures

Principles of coupling between flexible and rigid dynamics [27] are employed in this paper. The Craig–Bampton method is an established reduction technique in computational structural dynamics [28]. In this work, it is employed for reducing the physical d.o.f. for both the flexible support structure and the flexible rotating shaft. For both components, the d.o.f. are separated into retained and internal. The retained d.o.f. of the shaft are comprised of the interface d.o.f. between the shaft and the support structure, while the retained d.o.f. of the support structure

consist of the d.o.f. where boundary conditions are applied. All the remaining d.o.f. from each component are placed in the corresponding set of internal d.o.f. The application of the Craig–Bampton reduction method in the dynamic equations of the flexible support structure and of the flexible rotating shaft is described in this section.

2.1. Flexible dynamic response of support structure

The dynamic equations of motion for the support structure, modelled by the finite element method, are

$$[M^b]\{\ddot{x}^b\} + [C^b]\{\dot{x}^b\} + [K^b]\{x^b\} = \{F^b\}, \tag{1}$$

where $[M^b]$, $[C^b]$, $[K^b]$ and $\{F^b\}$ are the mass matrix, damping matrix, stiffness matrix and load vector, respectively. Superscript b denotes the support structure. The physical d.o.f. in the vector $\{x^b\}$ constitute the unknown variables.

Due to the large size of the vector $\{x^b\}$, the Craig–Bampton reduction method is employed. The initial displacement vector $\{x^b\}$ of Eq. (1) is partitioned into internal d.o.f. $\{x_i^b\}$ and retained d.o.f. $\{x_r^b\}$ (subscripts i and r, respectively). The vector $\{x_r^b\}$ consists of all the d.o.f. of the support structure at the locations where the flexible support structure is mounted. The vector $\{x_i^b\}$ includes all the remaining d.o.f. of vector $\{x^b\}$. Based on this partitioning, Eq. (1) is rewritten as

$$\begin{bmatrix} M_{ii}^b & M_{ir}^b \\ M_{ri}^b & M_{rr}^b \end{bmatrix} \begin{Bmatrix} \ddot{x}_i^b \\ \ddot{x}_r^b \end{Bmatrix} + \begin{bmatrix} C_{ii}^b & C_{ir}^b \\ C_{ri}^b & C_{rr}^b \end{bmatrix} \begin{Bmatrix} \dot{x}_i^b \\ \dot{x}_r^b \end{Bmatrix} + \begin{bmatrix} K_{ii}^b & K_{ir}^b \\ K_{ri}^b & K_{rr}^b \end{bmatrix} \begin{Bmatrix} x_i^b \\ x_r^b \end{Bmatrix} = \begin{Bmatrix} F_i^b \\ F_r^b \end{Bmatrix}. \tag{2}$$

The fixed-interface eigenvalues ω_j^2 and the corresponding eigenvectors $\{x_j\}$ are computed for the first J fixed-interface modes. Usually J is much smaller than the number of internal d.o.f. A set of static (or constraint) modes is introduced in order to account for the influence of the non-zero values of the retained d.o.f. $\{x_r^b\}$ on the internal d.o.f. $\{x_i^b\}$. The internal d.o.f. can be expressed as a linear superposition of the fixed-interface modes and the static modes so that the vector of the initial d.o.f. $\{x^b\}$ can be expressed in terms of a reduced basis comprised of the retained d.o.f. and the modal participation factors of the fixed-interface modes; i.e.

$$\{x^b\} = \begin{Bmatrix} x_i^b \\ x_r^b \end{Bmatrix} = \begin{bmatrix} X^b & Y^b \\ 0 & I \end{bmatrix} \begin{Bmatrix} \alpha^b \\ x_r^b \end{Bmatrix} = [\phi^b] \begin{Bmatrix} \alpha^b \\ x_r^b \end{Bmatrix}, \tag{3}$$

where

$$[\phi^b] = \begin{bmatrix} X^b & Y^b \\ 0 & I \end{bmatrix}, \qquad [Y^b] = -[K_{ii}^b]^{-1}[K_{ir}^b].$$

Matrix $[\phi^b]$ constitutes the modal matrix of the reduced basis of the Craig–Bampton d.o.f.

Substitution of Eq. (3) into Eq. (2) and pre-multiplication by the transpose of $[\phi^b]$ yields the following reduced system of equations:

$$[\bar{M}^b] \begin{Bmatrix} \ddot{\alpha}^b \\ \ddot{x}_r^b \end{Bmatrix} + [\bar{C}^b] \begin{Bmatrix} \dot{\alpha}^b \\ \dot{x}_r^b \end{Bmatrix} + [\bar{K}^b] \begin{Bmatrix} \alpha^b \\ x_r^b \end{Bmatrix} = \{\bar{F}^b\}, \tag{4}$$

where $[\bar{M}^b]$, $[\bar{C}^b]$and $\bar{K}^b$ are the reduced mass, damping and stiffness matrices, respectively, and

$$\{\bar{F}^b\} = [\phi^b]^{\mathrm{T}} \begin{Bmatrix} F_i^b \\ F_r^b \end{Bmatrix}$$

is the vector of the modal forces. The main computational benefit of the Craig–Bampton reduction process is that the size of the generalized co-ordinate vector $\{\alpha^b, x_r^b\}^{\mathrm{T}}$ is much smaller than the size of the vector containing the physical d.o.f. $\{x^b\}$.

2.2. Flexible dynamic response of shaft

Similar to the flexible support structure, the reduced equations of motion for the shaft are written as

$$[\bar{M}^c] \begin{Bmatrix} \ddot{\alpha}^c \\ \ddot{x}_r^c \end{Bmatrix} + [\bar{C}^c] \begin{Bmatrix} \dot{\alpha}^c \\ \dot{x}_r^c \end{Bmatrix} + [\bar{K}^c] \begin{Bmatrix} \alpha^c \\ x_r^c \end{Bmatrix} = \{\bar{F}^c\}, \tag{5}$$

where the matrices $[\bar{M}^c]$, $[\bar{C}^c]$and $[\bar{K}^c]$ in Eq. (5) are the reduced mass, damping and stiffness matrices, respectively, and $\{\bar{F}^c\}$ is the vector of the modal force. A modal matrix $[\phi^c]$, which is comprised of the fixed-interface modes and the static correction matrix from the physical matrices of the shaft, is utilized to get the reduced equations above (Eq. (5)). The Craig–Bampton d.o.f. $\{\alpha^c, x_r^c\}^{\mathrm{T}}$ contain the modal participation factors of the fixed-interface modes and the retained physical d.o.f. included in $\{x_r^c\}$. For one of the support locations, $\{x_r^c\}$ also includes the z d.o.f. of the center grid in order to apply an axial boundary condition (see Fig. 2). Finally, the y d.o.f. of two points on the outer surface of the shaft are also included in $\{x_r^c\}$ in order to impose an appropriate torsional boundary condition. A right-hand co-ordinate system xyz is used with the x- and z-axis pointing in the vertical and axial directions, respectively.

3. Coupled rigid and dynamic response of the shaft

An algorithm has been presented in the literature [12] for capturing the coupling effect between rigid-body rotation and flexible deformation for a rotating flexible shaft. The flexible dynamic behavior of the shaft is modelled by finite elements. A set of Craig–Bampton d.o.f. is used to

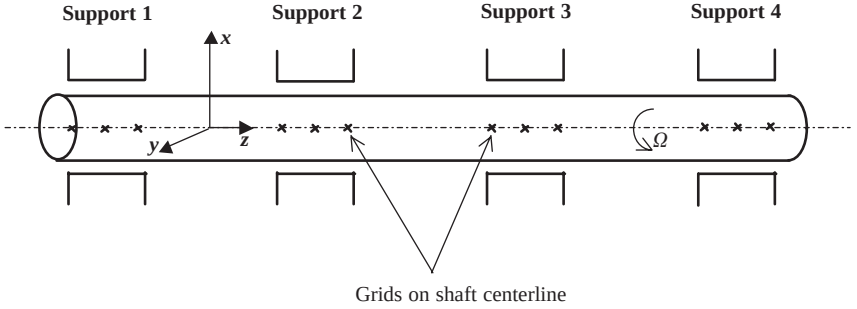

Fig. 2. Layout of a flexible shaft, its associated co-ordinate system, and its supports.

represent the flexible d.o.f. of the shaft [12]. This algorithm is employed in the present work. The Craig–Bampton d.o.f., defined in Section 2.2, are utilized. Thus, the vector of all the d.o.f. for the shaft becomes

$$\begin{Bmatrix} \theta \\ x^c \end{Bmatrix} = \begin{bmatrix} 1 & 0 & 0 \\ 0 & X^c & Y^c \\ 0 & 0 & I \end{bmatrix} \begin{Bmatrix} \theta \\ \alpha^c \\ x_r^c \end{Bmatrix} = [\bar{\Phi}^c] \begin{Bmatrix} \theta \\ \alpha^c \\ x_r^c \end{Bmatrix} = [\bar{\Phi}^c] \begin{Bmatrix} \theta \\ \eta^c \end{Bmatrix} = [\Phi^c]\{q^c\}, \tag{6}$$

where

$$\{\eta^c\} = \begin{Bmatrix} \alpha^c \\ x_r^c \end{Bmatrix}, \qquad [\bar{\phi}^c] = \begin{bmatrix} 1 & 0 \\ 0 & \phi^c \end{bmatrix} = \begin{bmatrix} 1 & 0 & 0 \\ 0 & X^c & Y^c \\ 0 & 0 & I \end{bmatrix}.$$

The shaft equations of motion including the rigid-body rotation effect are given as

$$\begin{bmatrix} M_{\theta\theta} & M_{\theta f}^c \\ sym. & M_{ff}^c \end{bmatrix} \begin{Bmatrix} \ddot{\theta} \\ \ddot{x}^c \end{Bmatrix} + \begin{bmatrix} 0 & 0 \\ 0 & C_{ff}^c \end{bmatrix} \begin{Bmatrix} \dot{\theta} \\ \dot{x}^c \end{Bmatrix} + \begin{bmatrix} 0 & 0 \\ 0 & K_{ff}^c \end{bmatrix} \begin{Bmatrix} \theta \\ x^c \end{Bmatrix} = \{Q_v^c\} + \{Q_e^c\}, \tag{7}$$

where θ is the rigid-body rotation, $\{x^c\}$ the all physical nodal flexible d.o.f. of the shaft, $[C_{ff}^c]$ and $[K_{ff}^c]$ the finite element damping and stiffness matrices, respectively, $\{Q_v^c\}$ a quadratic velocity vector that contains the effects of centrifugal and Coriolis forces, and $\{Q_e^c\}$ the vector of generalized external forces. In Eq. (7) all the terms are expressed with respect to the global co-ordinate system and are derived from assembling the corresponding element quantities. The quadratic velocity vector for a finite element is

$$\{Q_v^e\} = \begin{Bmatrix} -2\{e\}^{\mathrm{T}}[Y^e]\{\dot{e}_f\}\dot{\theta} \\ [Y^e]\{e\}\dot{\theta}^2 + 2[H^e]\{\dot{e}_f\}\dot{\theta} + [Y^e]\{e_f\}\dot{\theta}^2 \end{Bmatrix}. \tag{8}$$

The $[Y^e]\{e\}\dot{\theta}^2$ and $2[H^e]\{\dot{e}_f\}\dot{\theta}$ terms represent the centrifugal and Coriolis forces, respectively. The term $[Y^e]\{e_f\}\dot{\theta}^2$ originates from considering the work done by the centrifugal forces. $\{e_f\}$ is the nodal displacement vector of a finite element and $\{e\}$ is the nodal co-ordinate vector of the deformed finite element. The vector of generalized external forces for a finite element is

$$\{Q_e^e\} = \begin{Bmatrix} \{e\}^{\mathrm{T}}[N]^{\mathrm{T}}[A_\theta]^{\mathrm{T}}\{A\}\{F^c\} \\ [N]^{\mathrm{T}}\{F^c\} \end{Bmatrix}, \tag{9}$$

where $\{F^c\}$ includes the externally applied forces on each physical d.o.f. of the shaft finite element model. In Eqs. (8) and (9), subscripts v and e denote the quadratic velocity vector and the external force vector, respectively. Assembly of all element vectors $\{Q_v^e\}$ and $\{Q_e^e\}$ results in the quadratic velocity vector $\{Q_v^c\}$ and the vector of generalized forces $\{Q_e^c\}$, respectively.

Substitution of Eq. (6) into Eq. (7) and pre-multiplication by $[\bar{\Phi}^c]^{\mathrm{T}}$ yields

$$[\bar{M}^c]\{\ddot{q}^c\} + [\bar{C}^c]\{\dot{q}^c\} + [\bar{K}^c]\{q^c\} = \{\bar{Q}^c\}. \tag{10}$$

Eq. (10) is the equations of motion that couple the rigid-body rotation and flexible deformation of the shaft. The mass, damping and stiffness matrices of the flexible-body, as well as the load vector are first computed at the element level, based on a three-dimensional solid finite element formulation. Then, the element matrices and vectors are assembled in order to generate the

corresponding global matrices and vectors. The reduced equations (10) are formed after the modal transformation matrix $[\bar{\Phi}^c]$ is computed.

4. Shaft–support structure interaction

4.1. Support clearance

The rotating shaft is supported by a flexible base structure. The supporting mechanism between the rotating flexible shaft and the flexible basis is represented by three sets of non-linear springs at each support location. The non-linear springs are connecting the centerline points of the shaft with points on the inner surface of the flexible support (Figs. 3 and 4). The non-linear springs offer support in the radial direction without restricting the rotation of the shaft.

The force of each non-linear spring is a function of the clearance distribution $h(z, \phi, t)$ between the outer surface of the shaft and the inner surface of the support structure. In this section, a relationship for h is derived as a function of the generalized co-ordinates of the supporting structure (Eq. (4)) and the shaft (Eq. (5)).

The shaft deformation is governed by its elastic curve (deformation of its centerline). Due to the high local rigidity of the shaft, its cross-sectional geometry is assumed to stay circular before and

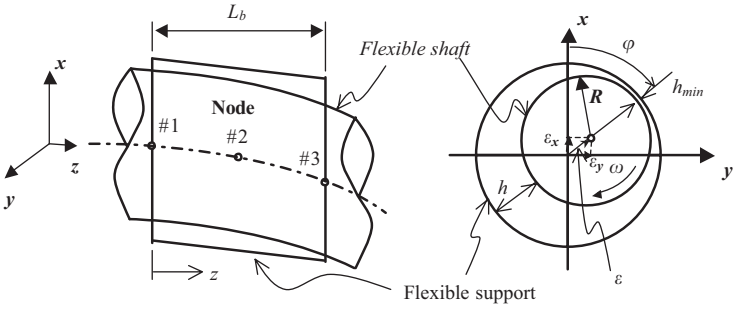

Fig. 3. Support configuration between flexible shaft and flexible basis.

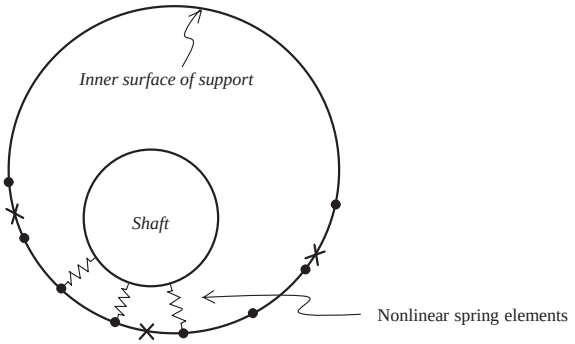

Fig. 4. Connection between shaft and support structure: ●, calculation grid point; x, physical grid point.

after deformation. Since the length of each support is relatively short, the deformation ε of the shaft centerline along each support (see Fig. 3) is considered to be quadratic. For each support, the deformations ε_1, ε_2 and ε_3 at the left end, middle and right end locations are used to define the shaft deformation distribution $\varepsilon(z)$ along the support length as

$$\varepsilon(z) = c_1 z^2 + c_2 z + c_3. \tag{11}$$

The constants c_1, c_2 and c_3 can be expressed in terms of ε_1, ε_2 and ε_3. Therefore, Eq. (11) can be rewritten as

$$\varepsilon(z) = A_1(z)\varepsilon_1 + A_2(z)\varepsilon_2 + A_3(z)\varepsilon_3, \tag{12}$$

where

$$A_1(z) = 2\left(\frac{z}{L_b}\right)^2 - 3\left(\frac{z}{L_b}\right) + 1, \qquad A_2(z) = -4\left(\frac{z}{L_b}\right)^2 + 4\left(\frac{z}{L_b}\right),$$
$$A_3(z) = 2\left(\frac{z}{L_b}\right)^2 - \left(\frac{z}{L_b}\right), \tag{13}$$

where L_b is the length of the support. Assuming temporarily that the support structure is undeformed, the clearance distribution between the outer surface of the shaft and the inner surface of the support can be expressed as [26]

$$h_r = c - \varepsilon_x \cos\varphi - \varepsilon_y \sin\varphi, \tag{14}$$

where, as shown in Fig. 3,

$$\varphi = \tan^{-1}(\varepsilon_y/\varepsilon_x). \tag{15}$$

The quantity c represents the original radial clearance at the undeformed state, and ε_x and ε_y represent the shaft deformations in the x and y directions, respectively. Substitution of Eq. (12) into Eq. (14) yields

$$h_r = c - [A_1(z) \quad A_2(z) \quad A_3(z)]\cos\varphi \begin{Bmatrix} \varepsilon_{x_1} \\ \varepsilon_{x_2} \\ \varepsilon_{x_3} \end{Bmatrix} - [A_1(z) \quad A_2(z) \quad A_3(z)]\sin\varphi \begin{Bmatrix} \varepsilon_{y_1} \\ \varepsilon_{y_2} \\ \varepsilon_{y_3} \end{Bmatrix}$$
$$= c - [T_c]\{x_c\}, \tag{16}$$

where ε_{x_i} and ε_{y_i}, $i = 1, 2, 3$ are the shaft deformations at node i in the x and y directions, respectively (see Fig. 3). The transformation matrix $[T_c]$ in Eq. (16) is

$$[T_c] = [A_1(z)\cos\varphi \quad A_1(z)\sin\varphi \quad A_2(z)\cos\varphi \quad A_2(z)\sin\varphi \quad A_3(z)\cos\varphi \quad A_3(z)\sin\varphi] \tag{17}$$

and

$$\{x_c\} = \{\, \varepsilon_{x_1} \quad \varepsilon_{y_1} \quad \varepsilon_{x_2} \quad \varepsilon_{y_2} \quad \varepsilon_{x_3} \quad \varepsilon_{y_3} \,\}^{\mathrm{T}}. \tag{18}$$

The above vector $\{x_c\}$ is a part of the retained d.o.f. vector $\{x_r^c\}$ of the shaft (see Eq. (6)).

A large number of non-linear spring elements are used in the circumferential direction (Fig. 4). Each non-linear spring element connects a node on the axis of the shaft with a point on the inner surface of the support. The force–displacement relationship of the spring element depends on the clearance between the inner surface of the support and the outer surface of the shaft. Since the

cross-section of the shaft retains its circular shape during the flexible deformation, the force–displacement relationship depends on the distance between the grid point on the shaft centerline and the inner surface of the support.

The deformation of any point on the outer surface of the shaft is calculated from Eq. (16) as a function of the shaft centerline deformations ε_x and ε_y at the left end, middle and right end of the support and as a function of the cylindrical co-ordinates (φ, z). According to Eq. (3), the deformation (δ_x, δ_y) of a physical grid point on the inner surface of the support in the x and y directions, respectively, is given by

$$\begin{Bmatrix} \delta_x \\ \delta_y \end{Bmatrix} = [\, X^b \quad Y^b \,] \begin{Bmatrix} \alpha^b \\ x_r^b \end{Bmatrix}, \tag{19}$$

where $\{\, \alpha^b \quad x_r^b \,\}^{\mathrm{T}}$ are the generalized co-ordinates of the support structure. Note that any grid point on the inner surface of the support belongs to the vector of internal d.o.f. $\{x_i^b\}$. Any point on the inner surface of the support, which belongs to the finite element mesh of the support structure, is considered as a physical grid point (see Fig. 4). The number of physical grid points at any cross-section of the support that are needed to capture the structural deformation of the support structure, is usually much smaller than the number of non-linear spring elements required to provide proper support for the rotating shaft. Therefore, a set of calculation grid points is used as shown in Fig. 4. The calculation grid points are placed at the locations of the non-linear spring elements and are utilized only for calculating the clearance between the shaft and the support.

The deformation of a calculation grid point in the x and y directions, respectively, is given by

$$\begin{Bmatrix} \delta_x \\ \delta_y \end{Bmatrix} = \begin{bmatrix} X_m & Y_m \end{bmatrix} \begin{Bmatrix} \alpha^b \\ x_r^b \end{Bmatrix}, \tag{20}$$

where the transformation matrix $[\, X_m \quad Y_m \,]$ is obtained through a cubic spline interpolation from the transformation matrix $[\, X^b \quad Y^b \,]$. The radial deformation δ of the support is

$$\delta = \delta_x \cos\psi + \delta_y \sin\psi = [\, \cos\psi \quad \sin\psi \,] \begin{Bmatrix} \delta_x \\ \delta_y \end{Bmatrix}, \tag{21a}$$

where

$$\psi = \tan^{-1}\left(\frac{\delta_y}{\delta_x}\right). \tag{21b}$$

Substitution of Eq. (20) into Eq. (21a) yields

$$\delta = [T_b] \begin{Bmatrix} \alpha^b \\ x_r^b \end{Bmatrix} = [T_b]\{x_b\}, \tag{22}$$

where

$$[T_b] = [\, \cos\psi \quad \sin\psi \,]\ [\, X_m \quad Y_m \,], \quad \{x_b\} = \begin{Bmatrix} \alpha^b \\ x_r^b \end{Bmatrix}, \tag{23}$$

Based on Eqs. (16) and (22), the clearance h between the shaft and the support is derived in cylindrical co-ordinates as

$$h(z,\varphi) = h_r + \delta = c - [T_c]\{x_c\} + [T_b]\{x_b\}. \tag{24}$$

Eq. (24) is utilized for determining the interaction forces that are created by the non-linear springs between the flexible support structure and the flexible rotating shaft. The interaction forces provide the coupling mechanism between the two components.

4.2. Combined dynamic equations for the shaft and the support structures

The equations for the flexible dynamic response of the support structure and the coupled rigid and flexible dynamic response of the shaft have been presented in Sections 2 and 3, respectively. The dynamic equations for the combined shaft and support structure system are derived in this section. The interaction between the shaft and the support structure is modelled by non-linear spring elements (Fig. 4). Combining Eqs. (1) and (7) results in

$$\begin{bmatrix} M^c_{\theta\theta} & M^c_{\theta f} & 0 \\ M^c_{f\theta} & M^c_{ff} & 0 \\ 0 & 0 & M^b_{ff} \end{bmatrix} \begin{Bmatrix} \ddot{\theta} \\ \ddot{x}^c \\ \ddot{x}^b \end{Bmatrix} + \begin{bmatrix} 0 & 0 & 0 \\ 0 & C^c_{ff} & 0 \\ 0 & 0 & C^b_{ff} \end{bmatrix} \begin{Bmatrix} \dot{\theta} \\ \dot{x}^c \\ \dot{x}^b \end{Bmatrix} + \begin{bmatrix} 0 & 0 & 0 \\ 0 & K^c_{ff} & 0 \\ 0 & 0 & K^b_{ff} \end{bmatrix} \begin{Bmatrix} \theta \\ x^c \\ x^b \end{Bmatrix} = \{Q_e\} + \{Q_v\} + \{Q\}, \tag{25}$$

where $\{Q\}$ is the vector of the physical non-linear spring forces applied both on the shaft and on the support structure. The vector $\{Q\}$ is a function of the clearance h between the shaft and the support. Superscripts c and b denote the shaft and support structure, respectively. Furthermore, subscripts θ and f denote the rigid-body rotation and the flexible deformation, respectively. The generalized external forces vector $\{Q_e\}$ and the quadratic velocity vector $\{Q_v\}$ [12] are

$$\{Q_e\} = \begin{Bmatrix} Q_{e\theta} \\ Q^c_{ef} \\ Q^b_{ef} \end{Bmatrix} = \begin{Bmatrix} (x^c + x^c_0)^{\mathrm{T}} N^{\mathrm{T}} A^{\mathrm{T}}_{\theta} A F^c \\ N^{\mathrm{T}} F^c \\ 0 \end{Bmatrix} \tag{26}$$

and

$$\{Q_v\} = \begin{Bmatrix} Q_{v\theta} \\ Q^c_{vf} \\ Q^b_{vf} \end{Bmatrix} = \begin{Bmatrix} -2(x^c + x^c_0)^{\mathrm{T}} Y^c \dot{x}^c \dot{\theta} \\ Y^c (x^c + x^c_0)\dot{\theta}^2 + 2H^c \dot{x}^c \dot{\theta} + Y^c x^c \dot{\theta}^2 \\ 0 \end{Bmatrix}. \tag{27}$$

Note that in Eqs. (25)–(27),

$$\{x^c\} = \mathop{\mathrm{A}}_{e=1}^{NM} \{e_f\}, \quad \{x^c_0\} = \mathop{\mathrm{A}}_{e=1}^{NM} \{e_0\}, \quad \{x^c_0\} = \mathop{\mathrm{A}}_{e=1}^{NM} \{e_0\}, \quad [Y^c] = \mathop{\mathrm{A}}_{e=1}^{NM} [Y^e],$$

$$[H^c] = \mathop{\mathrm{A}}_{e=1}^{NM} [H^e],$$

where the notation $\mathop{\mathrm{A}}_{e=1}^{NM}$ indicates assembly of element quantities over all the elements. The vector $\{x^c_0\}$ represents the physical nodal co-ordinates of the undeformed shaft, and the vector $\{F^c\}$

indicates the external forces on the shaft in the body co-ordinate system. By defining

$$[\Phi] = \begin{bmatrix} 1 & 0 & 0 \\ 0 & \bar{\phi}^c & 0 \\ 0 & 0 & \phi^b \end{bmatrix}, \tag{28}$$

the vector of the d.o.f. in Eq. (25) can be written as

$$\begin{Bmatrix} \theta \\ x^c \\ x^b \end{Bmatrix} = [\Phi]\{q\}, \tag{29a}$$

where

$$\{q\} = \{\, \theta \quad x_1 \quad x_c \quad x_b \,\}^{\mathrm{T}}. \tag{29b}$$

Substitution of Eq. (29a) into Eq. (25) and pre-multiplication by $[\Phi]^{\mathrm{T}}$ yields the following reduced system of equations:

$$[\bar{M}]\{\ddot{q}\} + [\bar{C}]\{\dot{q}\} + [\bar{K}]\{q\} = \{\bar{Q}_e\} + \{\bar{Q}_v\} + \{\bar{Q}\}. \tag{30}$$

The reduced mass matrix $[\bar{M}]$ is given by

$$[\bar{M}] = \begin{bmatrix} M^c_{\theta\theta} & (\bar{M}^c_{\theta f})_1 & (\bar{M}^c_{\theta f})_c & 0 \\ (\bar{M}^c_{\theta f})_1^{\mathrm{T}} & (\bar{M}^c_{ff})_{11} & (\bar{M}^c_{ff})_{1c} & 0 \\ (\bar{M}^c_{\theta f})_c^{\mathrm{T}} & (\bar{M}^c_{ff})_{1c}^{\mathrm{T}} & (\bar{M}^c_{ff})_{cc} & 0 \\ 0 & 0 & 0 & \bar{M}^b_{ff} \end{bmatrix}, \tag{31}$$

where

$$\begin{bmatrix} (\bar{M}^c_{ff})_{11} & (\bar{M}^c_{ff})_{1c} \\ (\bar{M}^c_{ff})_{1c}^{\mathrm{T}} & (\bar{M}^c_{ff})_{cc} \end{bmatrix} = [\bar{\phi}^c]^{\mathrm{T}}[M^c_{ff}][\bar{\phi}^c], \tag{32a}$$

$$\{\, (\bar{M}^c_{\theta f})_1 \quad (\bar{M}^c_{\theta f})_c \,\} = [M^c_{\theta f}][\bar{\phi}^c], \tag{32b}$$

$$[\bar{M}^b_{ff}] = [\bar{\phi}^b]^{\mathrm{T}}[M^b_{ff}][\bar{\phi}^b]. \tag{32c}$$

The reduced stiffness matrix $[\bar{K}]$ in Eq. (30) is

$$[\bar{K}] = \begin{bmatrix} 0 & 0 & 0 & 0 \\ 0 & (\bar{K}^c_{ff})_{11} & (\bar{K}^c_{ff})_{1c} & 0 \\ 0 & (\bar{K}^c_{ff})_{1c}^{\mathrm{T}} & (\bar{K}^c_{ff})_{cc} & 0 \\ 0 & 0 & 0 & \bar{K}^b_{ff} \end{bmatrix}, \tag{33}$$

where the individual reduced matrices are given by expressions similar to Eqs. (32a) and (32c). A similar expression also holds for the reduced damping matrix $[\bar{C}]$. The dimension of matrices $[\bar{M}]$, $[\bar{K}]$, and $[\bar{C}]$ is much smaller than that of matrices $[M]$, $[K]$, and $[C]$. This constitutes a significant size reduction compared to the number of physical d.o.f. present in the two finite element models.

The generalized external forces vector $\{\bar{Q}_e\}$ and the generalized quadratic vector $\{\bar{Q}_v\}$ are

$$\{\bar{Q}_e\} = [\Phi]^{\mathrm{T}}\{Q_e\}, \quad \{\bar{Q}_v\} = [\Phi]^{\mathrm{T}}\{Q_v\}, \tag{34}$$

where $\{Q_e\}$ and $\{Q_v\}$ are given by Eqs. (26) and (27), respectively.

The generalized force vector $\{\bar{Q}\}$, produced by the non-linear springs is

$$\{\bar{Q}\} = [\Phi]^{\mathrm{T}}\{Q\} \quad \text{or} \quad \{\bar{Q}\} = \begin{Bmatrix} 0 \\ 0 \\ -T_c^{\mathrm{T}} \\ T_b \end{Bmatrix}\{Q\}. \tag{35}$$

Eq. (35) is derived from the transformation presented by Eq. (24) between the generalized co-ordinates $\{q\}$ (see Eq. (29b)) and the distribution of physical clearance h between the outer surface of the shaft and the inner surface of the support.

5. Numerical solution process

5.1. Numerical integration

In this section the numerical time integration algorithm, developed to solve the reduced system of equations of motion (Eq. (30)), is presented. The Newmark method [29], modified by a Newton–Raphson iteration [30] process within each time step, is employed. An iterative loop within each time step is necessary since the equations of motion contain non-linear terms in the mass matrix and the forcing vectors. Based on the Newmark time integration, the following relations hold for the primary variables between successive iterations and successive time steps:

$$\{q\}_{n+1}^{i+1} = \{\Delta q\}_{n+1}^{i} + \{\Delta q\}_{n+1}^{i+1}, \tag{36a}$$

$$\{\dot{q}\}_{n+1}^{i+1} = a_1(\{q\}_{n+1}^{i+1} - \{q\}_n) - a_3\{\dot{q}\}_n - a_4\{\ddot{q}\}_n, \tag{36b}$$

$$\{\ddot{q}\}_{n+1}^{i+1} = a_2(\{q\}_{n+1}^{i+1} - \{q\}_n) - a_5\{\dot{q}\}_n - a_6\{\ddot{q}\}_n, \tag{36c}$$

where subscript n indicates the time step and superscript i indicates the iteration number within the time step. The constants a_1 through a_6 depend on the Newmark parameters γ and β, and the selected time step Δt.

Due to the non-linear terms in the governing equations, a Newton–Raphson iteration loop is necessary within each time step during the time integration. The derivatives of the non-linear terms in the governing equations (Eq. (30)) with respect to the primary variables $\{q\}$ are required by the Newton–Raphson iterative solution process. Therefore, expressions for the derivatives of the following matrices must be derived:

$$[PF] = \frac{\partial}{\partial\{q\}}([\bar{M}]\{\ddot{q}\}), \qquad [B] = \frac{\partial\{\bar{Q}\}}{\partial\{q\}}, \qquad [P] = \frac{\partial\{\bar{Q}\}}{\partial\{\dot{q}\}}. \tag{37–39}$$

After some algebra, the above matrices are expressed as

$$[PF] = \begin{bmatrix} 0 & 2(\{x_0^c\} + [\bar{\phi}^c]\{\eta_c\})^{\mathrm{T}}[Y^c][\bar{\phi}^c]\ddot{\theta} - \{\ddot{\eta}_c\}^{\mathrm{T}}[\bar{\phi}^c]^{\mathrm{T}}[H^c][\bar{\phi}^c] & 0 \\ 0 & -[\bar{\phi}^c]^{\mathrm{T}}[H^c][\bar{\phi}^c]\ddot{\theta} & 0 \\ 0 & 0 & 0 \end{bmatrix}, \tag{40}$$

$$[B] = \begin{bmatrix} (\{x_0^c\} + [\bar{\phi}^c]\{\eta_c\})^{\mathrm{T}} N^{\mathrm{T}} A_\theta^{\mathrm{T}} A \dfrac{\partial\{F^c\}}{\partial\theta} & \{F^c\}^{\mathrm{T}} A^{\mathrm{T}} A_\theta N[\bar{\phi}^c] - 2\dot{\theta}\{\dot{\eta}_c\}^{\mathrm{T}}[\bar{\phi}^c]^{\mathrm{T}}[Y^c][\bar{\phi}^c] & 0 \\ [\bar{\phi}^c]^{\mathrm{T}} N^{\mathrm{T}} \dfrac{\partial\{F^c\}}{\partial\theta} & 2[\bar{\phi}^c]^{\mathrm{T}}[Y^c][\bar{\phi}^c]\dot{\theta}^2 + [TdQT] & 0 \\ 0 & 0 & 0 \end{bmatrix}, \tag{41}$$

and

$$[P] = \begin{bmatrix} -2(\{x_0^c\} + [\bar{\phi}^c]\{\eta_c\})^{\mathrm{T}}[Y^c][\bar{\phi}^c]\{\dot{\eta}_c\} & -2(\{x_0^c\} + [\bar{\phi}^c]\{\eta_c\})^{\mathrm{T}}[Y^c][\bar{\phi}^c]\dot{\theta} & 0 \\ 2[\bar{\phi}^c]^{\mathrm{T}}[Y^c](\{x_0^c\} + 2[\bar{\phi}^c]\{\eta_c\})\dot{\theta} + 2[\bar{\phi}^c]^{\mathrm{T}}[H^c][\bar{\phi}^c]\{\dot{\eta}_c\} & 2[\bar{\phi}^c]^{\mathrm{T}}[H^c][\bar{\phi}^c]\dot{\theta} & 0 \\ 0 & 0 & 0 \end{bmatrix}, \tag{42}$$

where

$$\{\eta_c\} = \begin{Bmatrix} x_1 \\ x_c \end{Bmatrix} \tag{43}$$

and

$$[T\,\mathrm{d}QT] = \begin{bmatrix} 0 \\ -T_c^{\mathrm{T}} \\ T_b^{\mathrm{T}} \end{bmatrix} \left[\frac{\partial\{Q\}}{\partial\{h\}} + \frac{\partial\{Q\}}{\partial\{\dot{h}\}}\right][0 \quad -T_c \quad T_b]. \tag{44}$$

The final linearized system of equations to be solved for $\{\Delta q_{n+1}^{i+1}\}$ at the $(n+1)$th time step of the Newmark time integration can be expressed as

$$[AK]_{n+1}^i \{\Delta q\}_{n+1}^{i+1} = \{R\}_{n+1}^i, \tag{45}$$

where

$$[AK]_{n+1}^i = a_2[\bar{M}]_{n+1}^i + a_1[\bar{C}] + [\bar{K}] + [PF]_{n+1}^i - a_1[P]_{n+1}^i - [B]_{n+1}^i \tag{46}$$

and

$$\{R\}_{n+1}^i = \{\bar{Q}\}_{n+1}^i + [\bar{M}]_{n+1}^i\{R_1\} - [P]_{n+1}^i\{R_2\} + [\bar{C}]\{R_3\} - [\bar{K}]\{q\}_{n+1}^i. \tag{47}$$

The vectors $\{R_1\}, \{R_2\}$ and $\{R_3\}$ in Eq. (47) are as follows:

$$\{R_1\} = a_2\{q\}_n + a_5\{\dot{q}\}_n + a_6\{\ddot{q}\}_n - a_2\{q\}_{n+1}^i, \tag{48}$$

$$\{R_2\} = a_1\{q\}_n + a_3\{\dot{q}\}_n + a_4\{\ddot{q}\}_n - a_1\{q\}_{n+1}^i + \{\dot{q}\}_{n+1}^i, \tag{49}$$

$$\{R_3\} = a_1\{q\}_n + a_3\{\dot{q}\}_n + a_4\{\ddot{q}\}_n - a_1\{q\}_{n+1}^i. \tag{50}$$

The solution of Eq. (45) provides the primary variable change, within each iteration, of the $(n+1)$th time step. The Newton–Raphson iterative process is repeated until convergence is achieved. The iteration is considered converged when the maximum absolute value of the increase of all the non-linear spring forces within an iteration is less than or equal to a certain small value. Then the solution process advances to the following time step and a new set of Newton–Raphson iterations is performed. For a steady state excitation, the Newmark time integration is terminated when the absolute value of the change of every non-linear spring force is less than 1% of the force itself over an entire cycle.

Table 1
The physical properties of the finite element models

	Support structure	Shaft
Number of finite elements	2752	1824
Number of physical d.o.f.	12,807	5775
Number of internal d.o.f.	12,798	5748
Number of retained d.o.f.	9	27
Number of internal modes	150	50
Frequency range of internal modes (Hz)	0 ~ 22,361	0 ~ 12,743
Natural frequency (Hz)	121	155
Number of Craig–Bampton d.o.f.	159	77

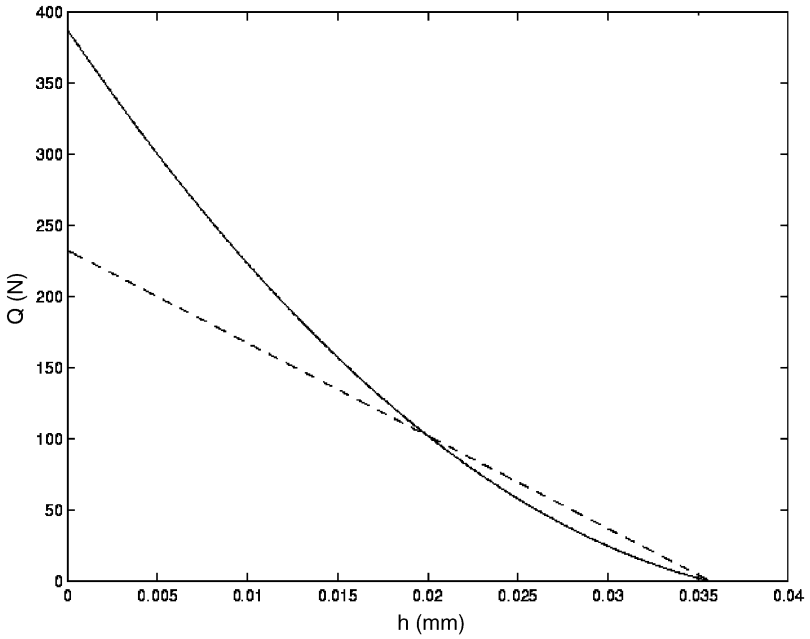

Fig. 5. $Q-h$ relation: ——, non-linear; ------, linear.

5.2. Computation of matrices

The finite element commercial code MSC/NASTRAN is utilized to compute the physical mass, damping and stiffness matrices of the finite element models of both the shaft and the support structure. A NASTRAN DMAP code is written to generate the transformation matrices in the

Table 2
The characteristics of analyses

Analyses	Load condition	Spring type	Rigid-body rotation
1	Static	Non-linear	No
2	Static	Non-linear	Yes
3	Sinusoidal	Non-linear	No
4	Sinusoidal	Linear	Yes
5	Sinusoidal	Non-linear	Yes

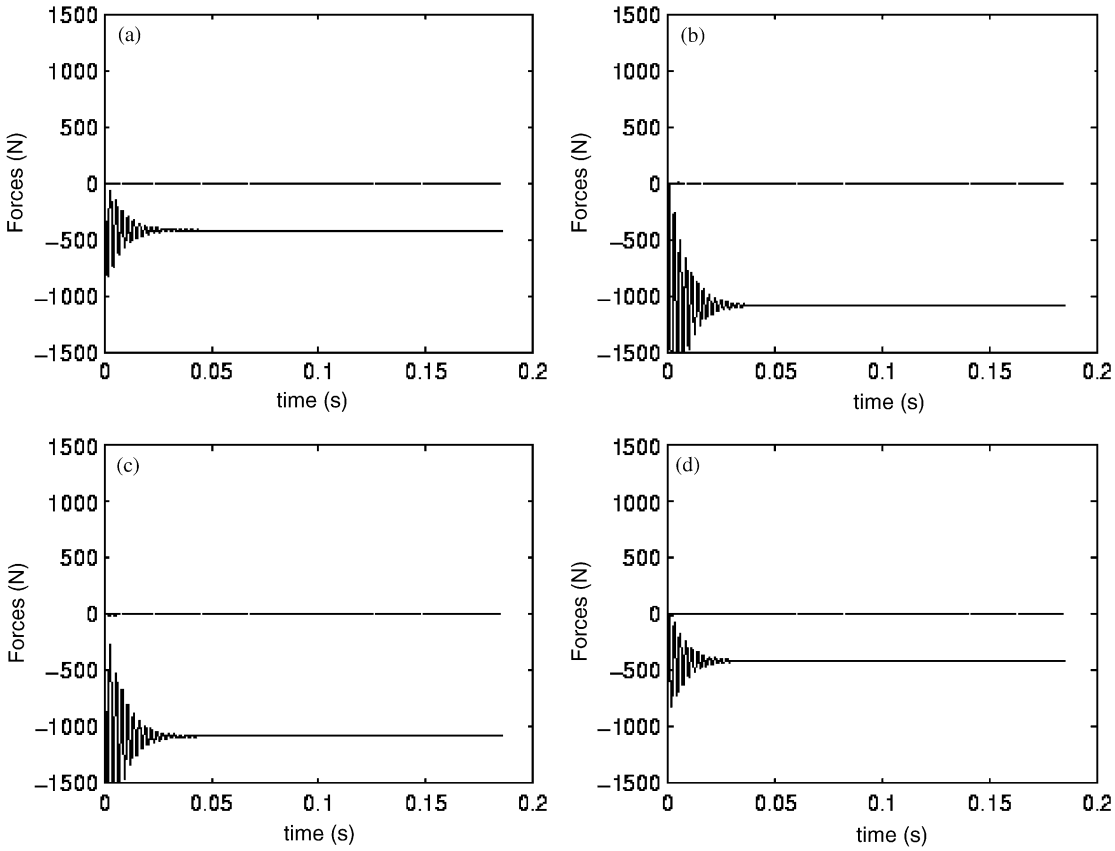

Fig. 6. Reaction forces at the supports for non-linear spring model without rigid-body rotation under static excitations: ——, RX; ------ RY; (a) support #1; (b) support #2; (c) support #3; (d) support #4.

Craig–Bampton basis $[\phi^b]$ and $[\phi^c]$ in Eqs. (3) and (5), respectively. The submatrices in $[\bar{M}]$, $[\bar{C}]$ and $[\bar{K}]$ in the reduced system of equations (Eq. (30)) that correspond to the Craig–Bampton d.o.f. are obtained by pre- and post-multiplying the mass, damping and stiffness matrices associated with the physical d.o.f. with the corresponding transformation matrices. This operation is performed in the DMAP code. Certain components of the derivative matrices $[PF]$, $[B]$, and $[P]$ in Eqs. (40)–(42), $([\bar{\phi}^c]^T[Y^c][\bar{\phi}^c]$, $[\bar{\phi}^c]^T[H^c][\bar{\phi}^c]$, $\{x_0^c\}^T[Y^c][\bar{\phi}^c])$, are also computed in the DMAP code. A specialized FORTRAN code collects all the arrays, assembles the final system of equations (Eq. (45)), and solves it for $\{\Delta q\}$ by the algorithm described in Section 5.1.

6. Analysis of a rotating shaft supported by a flexible base structure

A rotating shaft supported by a flexible structure is analyzed. The non-linear coupling between the rigid-body rotation and the flexible dynamics of the shaft is included in the analysis along with the non-linear interaction between the shaft and the support structure. The system has a simple geometry in order to validate the new development by comparing the results with expected trends due to the simple geometry.

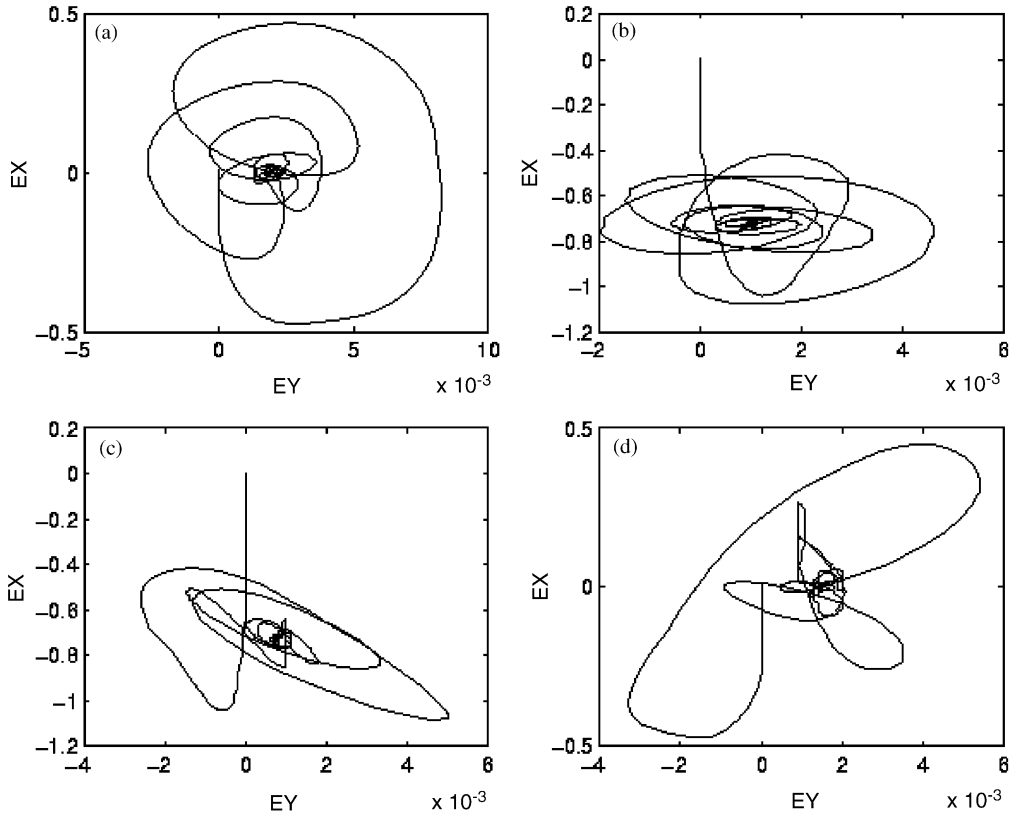

Fig. 7. Eccentricity for non-linear spring model without rigid-body rotation under static excitations: (a) support #1; (b) support #2; (c) support #3; (d) support #4.

6.1. Finite element modelling of shaft and support structure

As depicted in Fig. 1, the finite element model of the rotating shaft is supported at four locations by the flexible support structure. The shaft has a length of 1404 mm and a diameter of 68 mm. The support structure is 1381 mm in length and 50 mm in height. The length of each one of the four supports is 25 mm and the thickness of each support is 20 mm. The material for both the shaft and the support structure is steel with Young's modulus of 200 GPa and mass density of 7860 kg/m^3. The first non-zero natural frequency of the shaft under free boundary conditions is 155 Hz and the first non-zero natural frequency of the support structure under free boundary conditions is 121 Hz. The initial radial clearance between the outer surface of the shaft and the inner surface of the support is equal to 35.687 μm.

The finite element model of the base structure is comprised of 2752 finite elements and contains 12,807 physical d.o.f. On the top of the support structure, three nodes are chosen to be the mount nodes where all the translational d.o.f. are restrained (see Fig. 1). All the physical d.o.f. are partitioned into 12,798 internal d.o.f. and 9 retained d.o.f. The retained d.o.f. are the d.o.f. of all the mount nodes. A modal basis containing 150 modes is employed for representing the internal d.o.f. The 150 internal normal modes cover a frequency range from 0 to 22,361 Hz. Thus, the total number of the Craig–Bampton d.o.f. for the base structure is equal to 159. Similarly, the finite element model of the shaft is comprised of 1824 finite elements and contains 5775 physical d.o.f.

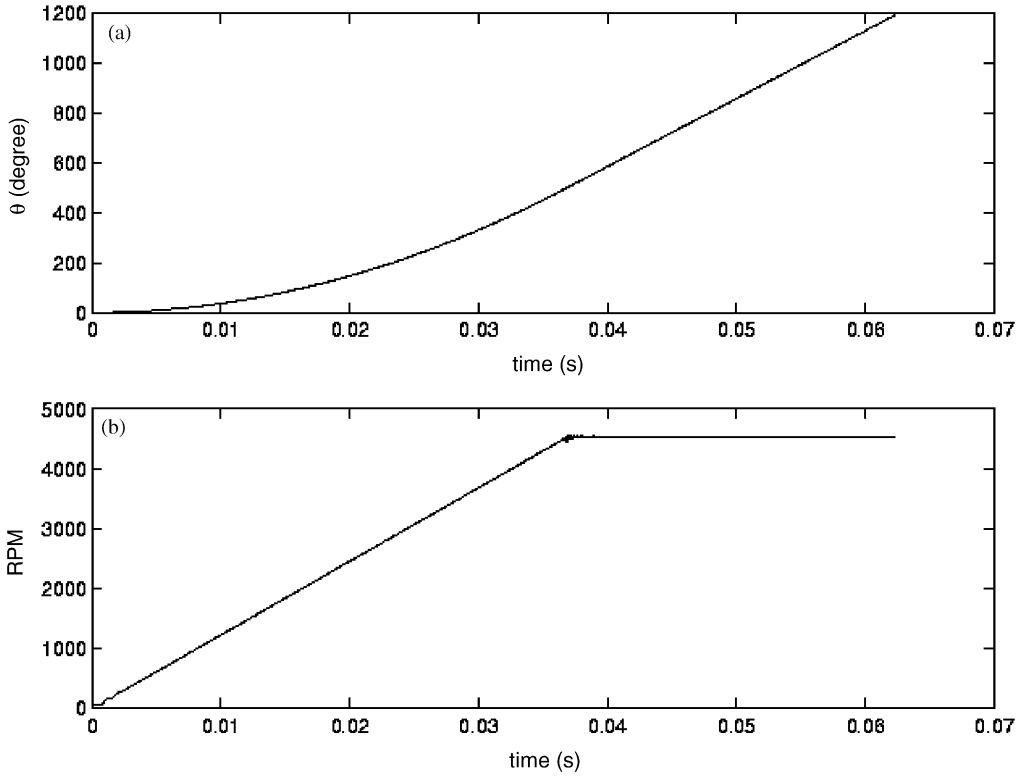

Fig. 8. Rigid body (a) rotation angle and (b) r.p.m.

The latter are partitioned into 5748 internal d.o.f. and 27 retained d.o.f. The retained d.o.f. of the shaft are the vertical and lateral d.o.f. of all the nodes on the centerline of the shaft inside each support location, plus the z d.o.f. of the center node inside the third support location, and the two lateral d.o.f. on the top and bottom nodes at one end of the shaft section. A model basis containing 50 modes representing the internal d.o.f. leads to a total number of 77 Craig–Bampton d.o.f. for the shaft. The frequency range covered by the 50 internal normal modes is from 0 to 12,743 Hz. The total number of the d.o.f .in vector $\{q\}$ for the system, including the rigid-body rotation d.o.f., is equal to 237, which is much smaller than the total physical d.o.f. of the two finite element models. The physical properties of the finite element models are summarized in Table 1.

6.2. *Analysis process*

In this example, the interaction between the shaft and the base structure is represented either by a set of linear springs or by a set of non-linear springs. For the linear springs, the relation between the force Q and the clearance h is

$$Q = \begin{cases} 233 - 6517h & \text{for} \quad h < c_0, \\ 0 & \text{for} \quad h > c_0, \end{cases} \tag{51}$$

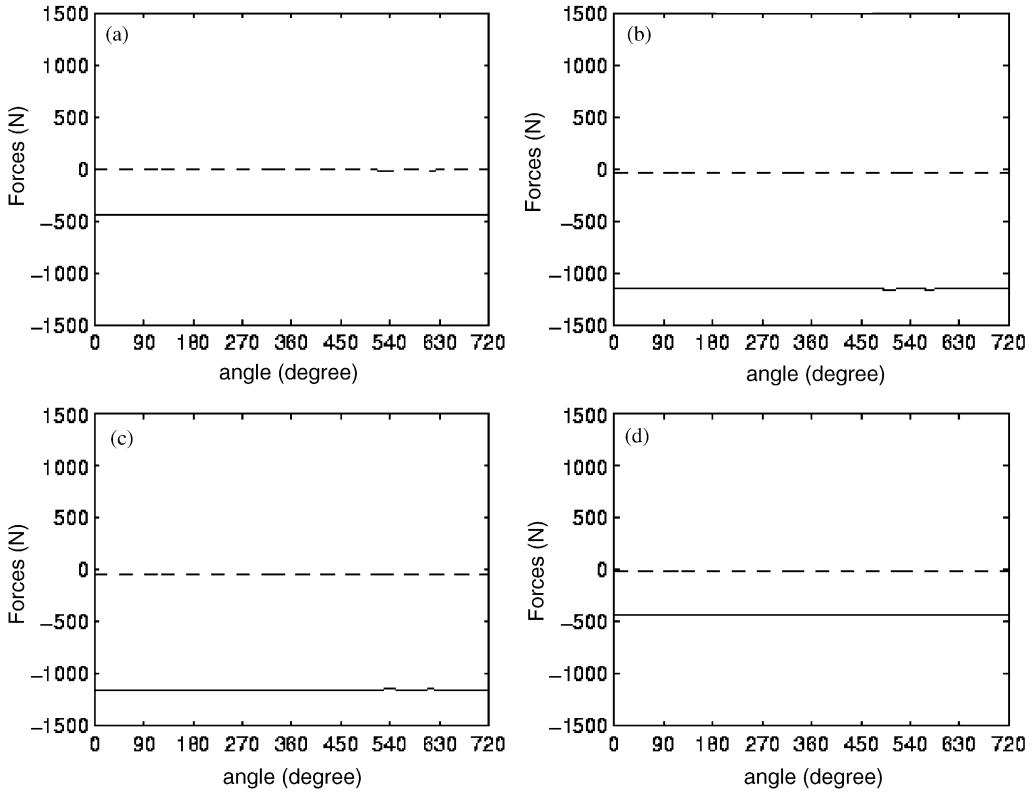

Fig. 9. Reaction forces at the supports for non-linear spring model with rigid-body rotation under static excitations: ——, RX; ------, RY; (a) support #1; (b) support #2; (c) support #3; (d) support #4.

where $c_0 = 0.035687$ mm is the initial clearance, and Q is in Newtons. The 'linear' relationship expressed by Eq. (51) is pseudo-linear since it represents compressive-only springs. For the non-linear springs, the force–clearance relation is

$$Q = \begin{cases} 388 - 18632h + 217550h^2 & \text{for } h < c_0, \\ 0 & \text{for } h > c_0. \end{cases} \tag{52}$$

The $Q - h$ relation is plotted in Fig. 5 for both linear and non-linear springs.

Two forces equal in magnitude with opposite directions are applied in the body co-ordinate system on a top and on a bottom grid at the end section of the shaft to generate an external torque. The external torque is applied on the shaft until the desired rotational speed is reached. Since there is no friction or resisting torque in this application, the shaft will continue to rotate at a desired constant speed once the external torque is removed. Three vertical loads are applied along the global X direction at the middle location in between the four supports. Since the non-linear behavior in the system is introduced from both the coupling between the rigid and the flexible d.o.f. of the shaft, and from the non-linear springs connecting the shaft and the base structure at the supports, five analyses are performed in order to gradually demonstrate the

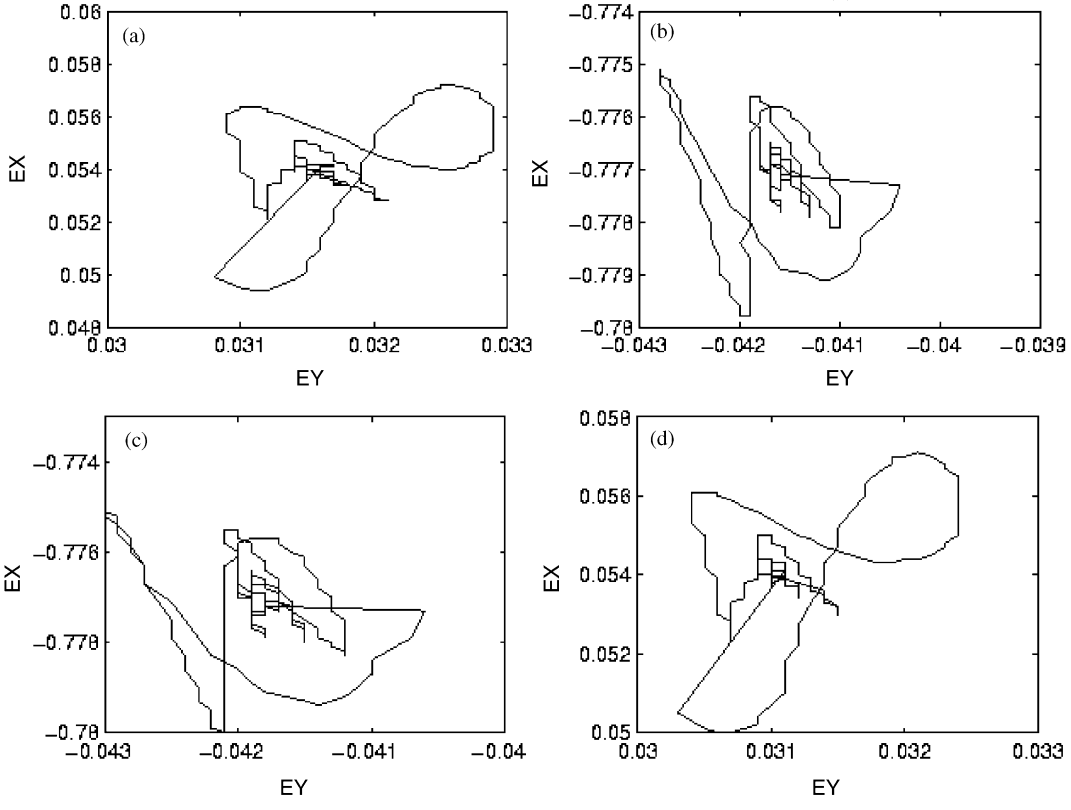

Fig. 10. Eccentricity for non-linear spring model with rigid-body rotation under static excitations: (a) support #1; (b) support #2; (c) support #3; (d) support #4.

validity and the capabilities of the new algorithm. For all the analyses the reaction forces at the supports and the eccentricity of the center node at each support location are presented. The nature of the external excitation, the type of springs utilized in the analysis, and the presence of a rigid-body rotation constitute the characteristics that vary between different analyses. The characteristics of each analysis are summarized in Table 2.

6.3. Computation results

First, three vertical static loads of 1000 N each and no torque are applied on the shaft, while the non-linear spring connection is considered between the shaft and the base. A time step of 7.4×10^{-5} s is employed in this analysis. The reaction forces at the supports with respect to time are presented in Fig. 6. As expected, since there is no coupling effect between the rigid-body rotation and the flexible dynamics, all the reaction forces in the lateral direction (Y direction) are equal to zero. The vertical forces in the X direction reach constant values once the transient effects are diminished. The sum of all the reaction forces is equal to the sum of all the external loads, and the expected symmetry is observed in the values of the forces. The eccentricity results are

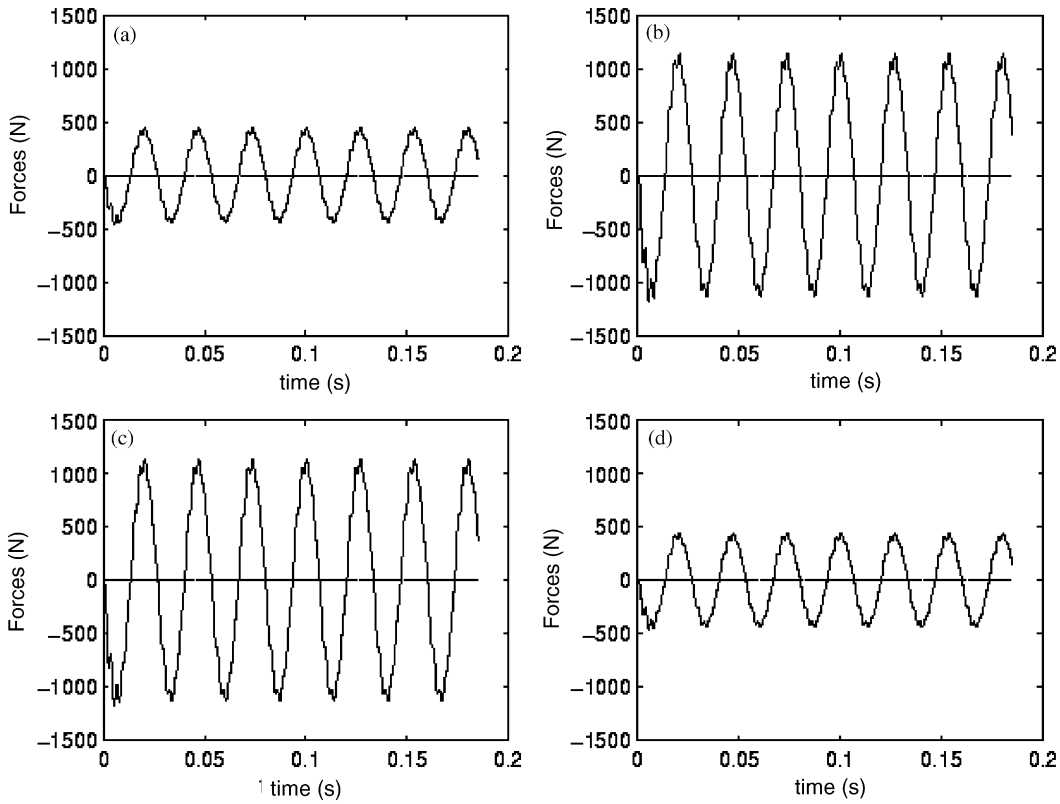

Fig. 11. Reaction forces at the supports for non-linear spring model without rigid-body rotation under sinusoidal excitations: ——, RX; ------, RY; (a) support #1; (b) support #2; (c) support #3; (d) support #4.

presented in Fig. 7. The deformation in the Y direction is practically equal to zero and symmetry is preserved in the X displacements at the supports as expected. In addition, multiplication of the induced deformation with the appropriate values of the non-linear springs (Fig. 5) results in the computed values of the reaction forces (Fig. 6). This first analysis verifies that the time integration algorithm and the non-linear interaction between the flexible shaft and the flexible support structure have been implemented properly in the developed software.

A constant rotational speed of 4500 r.p.m. is introduced in the first analysis. An external torque is applied on the shaft until the desired rotational speed of 4500 r.p.m. is reached and then the torque is removed. Fig. 8 presents the time history for the r.p.m. and the angle of rotation in the time range when the constant rotational speed is reached. It can be observed that as long as the torque is applied on the shaft the rotational speed increases linearly while a constant speed is retained once the external torque is removed. As expected, the angle of rotation varies linearly with time once the externally applied torque is released. The forces and the eccentricities at the supports are presented in Figs. 9 and 10, respectively. In this case, both sets of results are presented over the final 720° of rotation once convergence has been achieved. As expected,

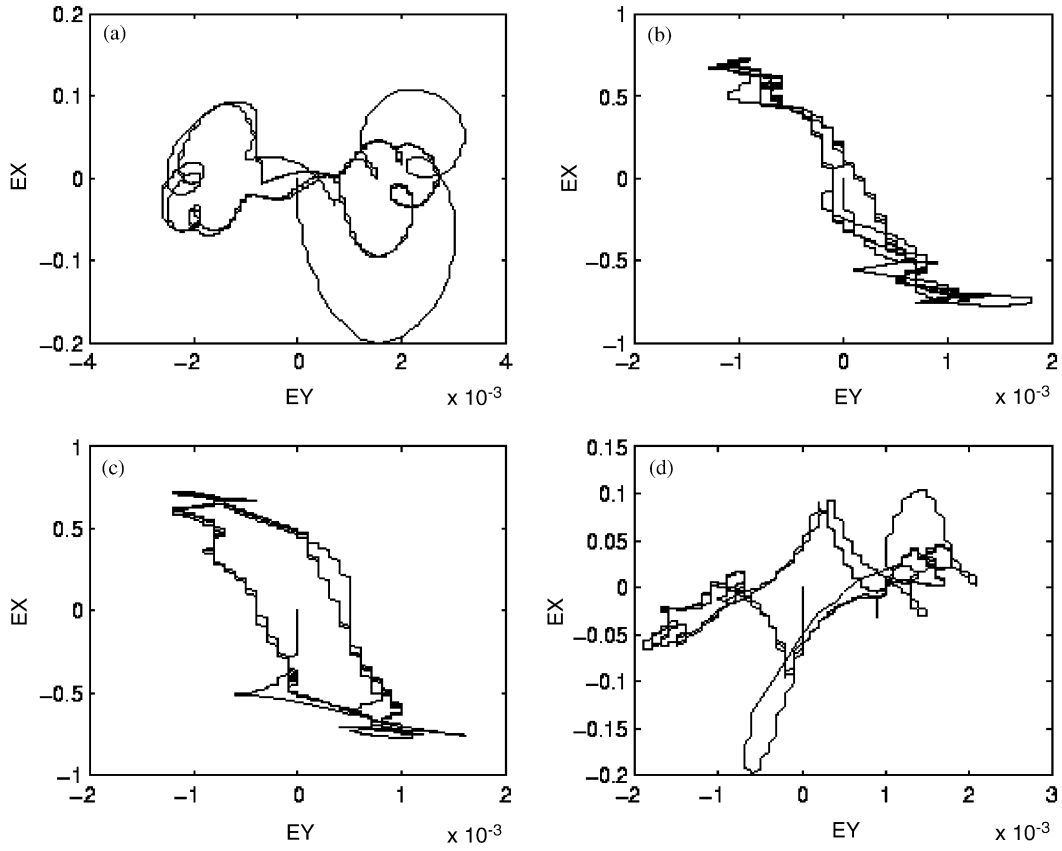

Fig. 12. Eccentricity for non-linear spring model without rigid-body rotation under sinusoidal excitations: (a) support #1; (b) support #2; (c) support #3; (d) support #4.

symmetry is observed in the results for both the reaction forces and the eccentricities. Due to the non-linear coupling between the rigid-body rotation and flexible deformation of the shaft, a small but not negligible eccentricity is introduced in the lateral Y direction. Thus, a small reaction force is also introduced at the supports in the Y direction. The forces at the supports are constant over time since the external vertical load is static. In addition, the values of the support forces are similar to the values computed by the previous analysis without rotation, since the influence of the non-linear coupling effect between rotational and flexible d.o.f. is expected to be small for a static external load. This analysis in conjunction with results presented in Ref. [12] demonstrates that the validity of the coupling between rigid- and flexible-body dynamics has been preserved during the coupling process between the flexible shaft and the flexible support structure.

In the third analysis, three sinusoidal excitations are introduced in order to replace the three static loads of the first analysis. The amplitude of all the harmonic loads is equal to 1000 N. The springs between the shaft and the supports are non-linear. No external torque is applied, thus no rotation is introduced in the shaft. The reaction forces at the supports with respect to time are presented in Fig. 11. Some transient effects can be observed during the first cycle while a steady state is achieved after that. As expected, since there is no coupling effect between the rigid-body rotation and the flexible dynamics, all the reaction forces in the lateral direction (Y direction) are

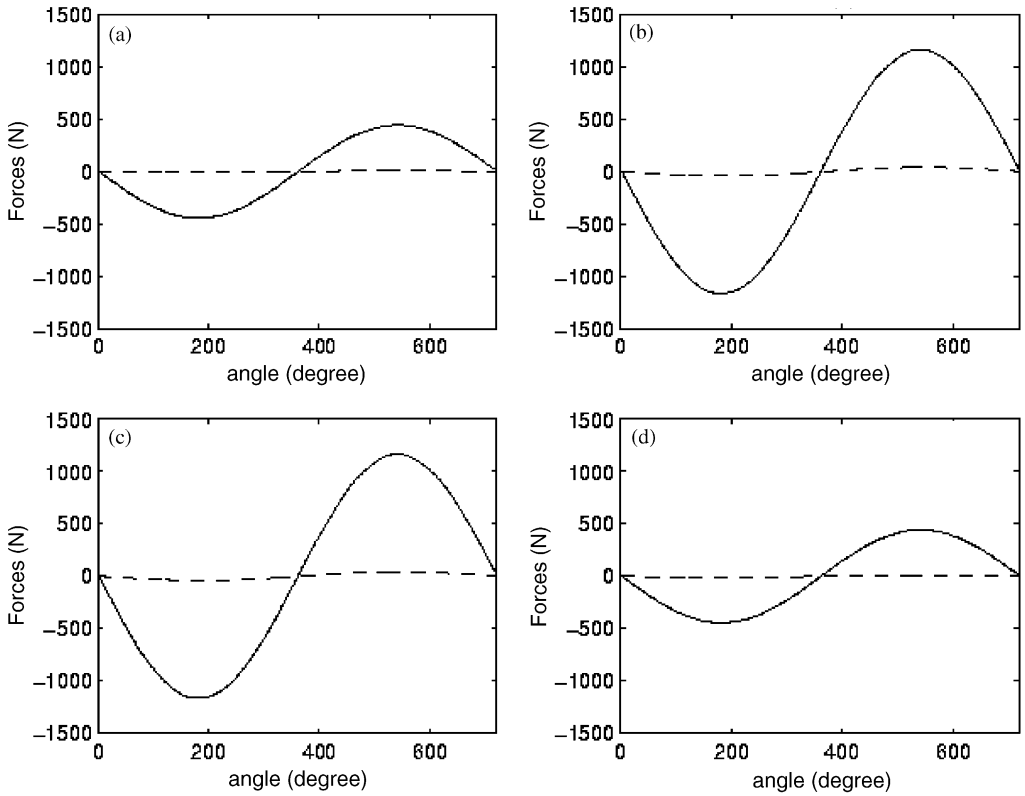

Fig. 13. Reaction forces at the supports for linear spring model with rigid-body rotation under sinusoidal excitations: ——, RX; ------, RY; (a) support #1; (b) support #2; (c) support #3; (d) support #4.

equal to zero. The vertical forces in the X direction are also sinusoidal and the sum of the magnitude of all the reaction forces is equal to the sum of the magnitude of all the external loads. The reactions at supports one and two are symmetric to the reaction forces at supports four and three, respectively. This is expected due to the symmetry of the structure and the symmetry of the external loads. The eccentricity results are presented in Fig. 12. As expected, the deformation in the Y direction is practically equal to zero and symmetry is preserved in the X displacements at the supports. This analysis verifies that the time integration algorithm and the non-linear interaction between the flexible shaft and the flexible support structure are implemented correctly to compute the dynamic responses of the system.

The non-linear springs of the previous analysis are replaced by linear springs in the fourth analysis, while a rotational speed of 4500 r.p.m. is introduced. In summary, linear springs connect the shaft and the support, while sinusoidal loads and a rigid-body rotation are applied on the shaft. The frequency of the sinusoidal loads is equal to 37.5 Hz, which results into one cycle of the sinusoidal loads within 720° of rotation of the shaft. Fig. 13 presents the support reaction forces for the last 720° of the rigid-body rotation once convergence has been achieved. Since the connecting springs are linear, smooth reaction forces are computed at all the supports. The amplitude of each reaction force is equal to the magnitude of the static reaction forces computed

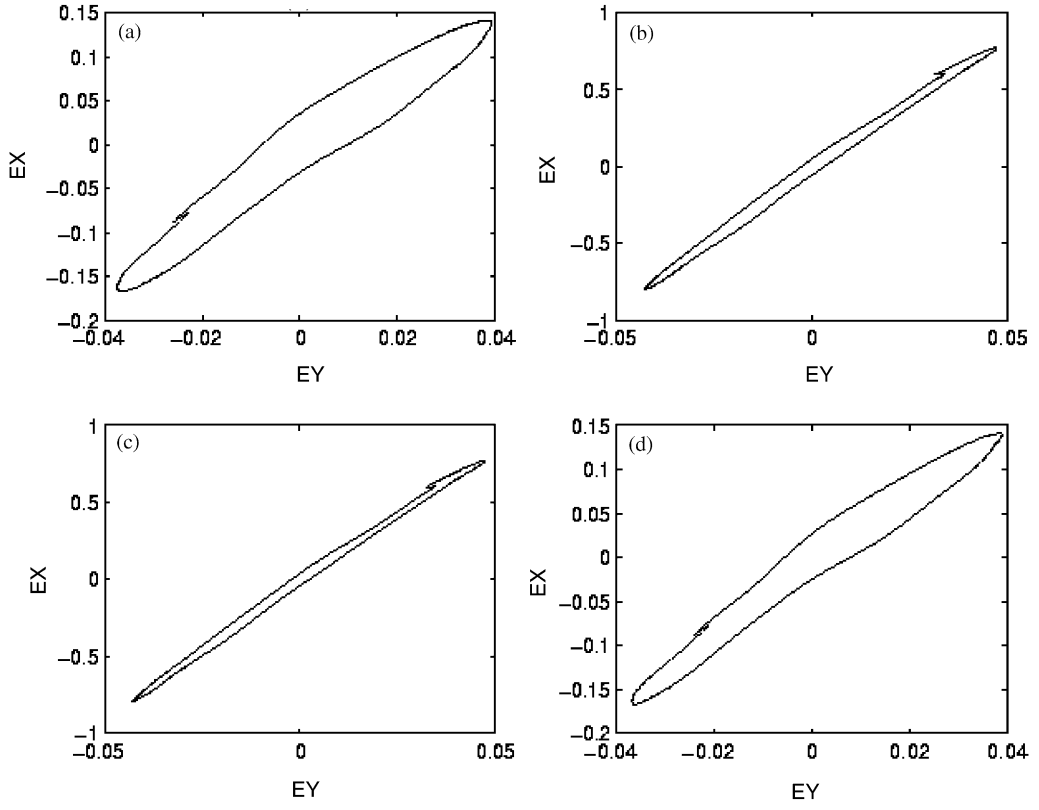

Fig. 14. Eccentricity for linear spring model with rigid-body rotation under sinusoidal excitations: (a) support #1; (b) support #2; (c) support #3; (d) support #4.

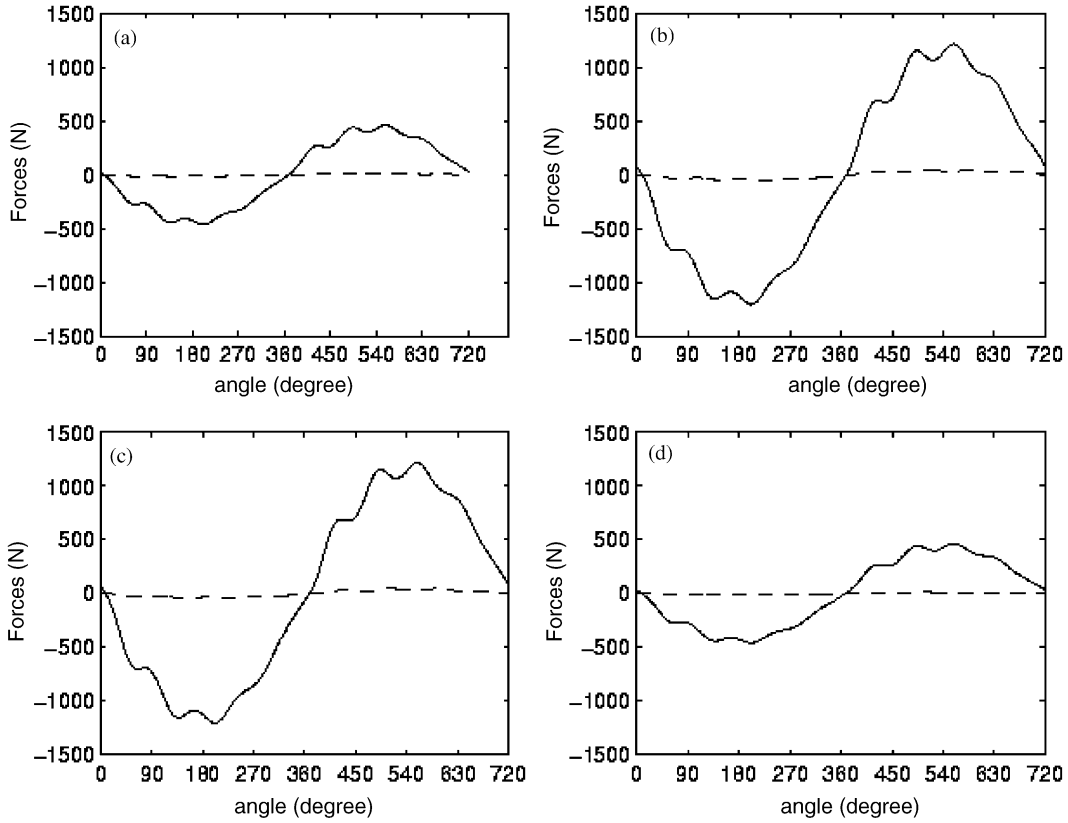

Fig. 15. Reaction forces at the supports for non-linear spring model with rigid-body rotation under sinusoidal excitations: ——, RX; ------, RY; (a) support #1; (b) support #2; (c) support #3; (d) support #4.

by the second analysis. Since there is non-linear coupling between the rigid-body rotation and the flexible deformation, small harmonic reaction forces in the Y direction for all four supports are observed, similar to the observations from the second analysis. The eccentricities for the last 720° of rotation are presented in Fig. 14. Four closed loops are obtained for the eccentricities, which indicates that in the last 720° of rotation, steady state has indeed been achieved. This result is expected since the location of the shaft at the end of a cycle comprises the location of the shaft at the start of the next cycle, due to the relationship between the frequency of the harmonic excitation and the rotational speed. The Y deformations are very small but not negligible, which is consistent with the observation made for the forces in the Y direction. Both the reaction forces and the eccentricities (Figs. 13 and 14) exhibit very good symmetry as expected.

In the last, fifth analysis, non-linear springs are used to replace the linear springs of the previous analysis while all other characteristics remain unchanged. The support reaction forces and eccentricities are presented in Figs. 15 and 16, respectively. Fig. 15 matches Fig. 13 in terms of the period and the amplitude of the response forces, however some fluctuations are observed in the reaction forces due to the non-linear nature of the springs. The eccentricity curves in Fig. 16 are also closed similar to results from the linear springs (Fig. 14). As expected, due to the non-linear

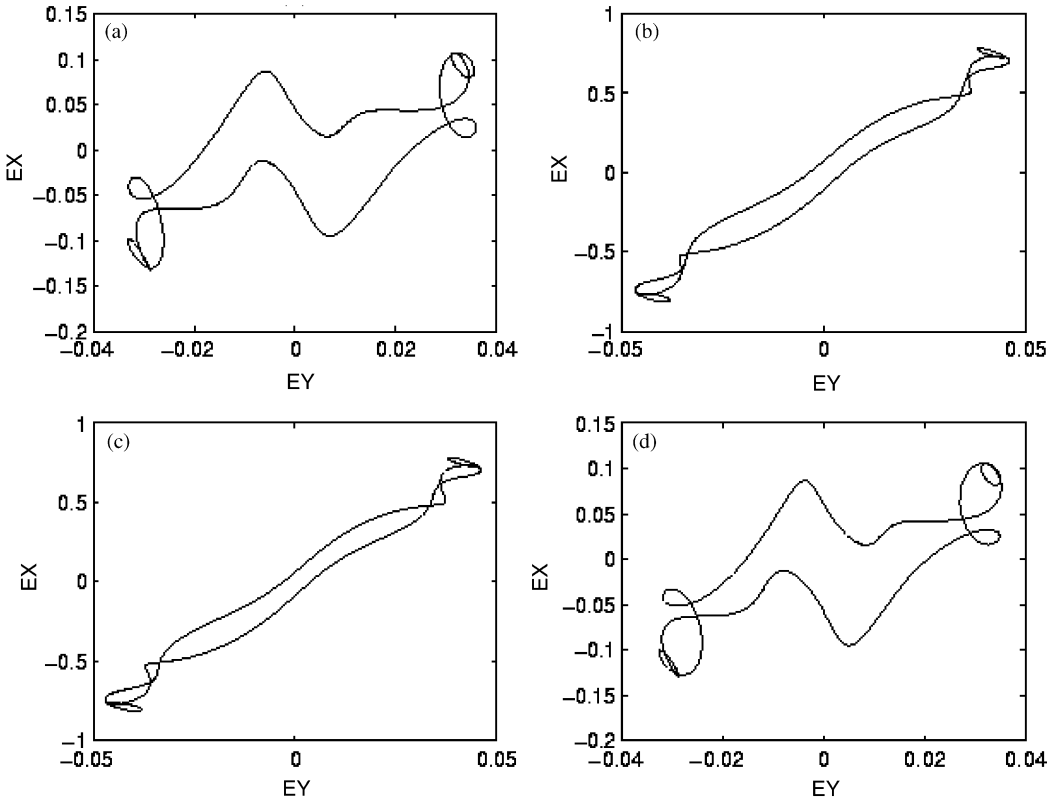

Fig. 16. Eccentricity for non-linear spring model with rigid-body rotation under sinusoidal excitations: (a) support #1; (b) support #2; (c) support #3; (d) support #4.

springs the eccentricity loops are not as smooth as the ones resulting from the linear springs (Fig. 14). Both reaction forces and eccentricities demonstrate symmetry due to the symmetric nature of the structure and the external loads.

7. Conclusions

A system approach is developed to formulate the dynamic response of a rotating shaft supported by a flexible support structure. The rigid- and flexible-body dynamics for the rotating shaft are included in the formulation. The shaft/support interaction is also considered and modelled by either linear or non-linear springs distributed around the circumference of the shaft. The support structure and the supports are considered flexible and the contribution from the flexible deformation to the clearance between the shaft and the support is included in the shaft/support interaction problem. The Craig–Bampton method is employed to condense the equations of motion. The final system of equation is non-linear and solved in time domain by the Newmark method modified by Newton–Raphson scheme. Analyses with different characteristics are performed and good results are obtained.

Acknowledgements

The completion of this work was made possible through support by NSF Grant No. CMS-9713793.

References

[1] T.R. Kane, R.R. Ryan, A.K. Banerjee, Dynamics of a cantilever beam attached to a moving base, Journal of Guidance, Control, and Dynamics 10 (2) (1987) 139–151.
[2] A. Yigit, R.A. Scott, A. Galip Ulsoy, Flexural motion of a radially rotating beam attached to a rigid body, Journal of Sound and Vibration 121 (2) (1988) 201–210.
[3] J.D. Downer, K.C. Park, J.C. Chiou, Dynamics of flexible beams for multibody systems: a computational procedure, Computer Methods in Applied Mechanics and Engineering 96 (1992) 373–408.
[4] J.W.-Z. Zu, R.P.S. Han, Natural frequencies and normal modes of a spinning Timoshenko beam with general boundary conditions, Journal of Applied Mechanics 59 (1992) 197–204.
[5] W.J. Hearing, R.R. Ryan, R.A. Scott, New formulation for flexible beams undergoing large overall plane motion, Journal of Guidance, Control, and Dynamics 17 (1) (1994) 76–83.
[6] D.J. Segalman, C.R. Dohrmann, A method for calculating the dynamics of rotating flexible structures, part 1: derivation, Journal of Vibration and Acoustics 118 (1996) 313–317.
[7] M.D. Al-Ansary, Flexural vibrations of rotating beams considering rotary inertia, Computers and Structures 69 (1998) 321–328.
[8] W. Pan, E.J. Haug, Flexible multibody dynamic simulation using optimal lumped inertia matrices, Computer Methods in Applied Mechanics and Engineering 173 (1999) 189–200.
[9] J. Mayo, J. Dominguez, A.A. Shabana, Geometrically nonlinear formulations of beams in flexible multibody dynamics, Journal of Vibration and Acoustics 117 (1995) 501–509.
[10] H. El-Absy, A.A. Shabana, Coupling between rigid body and deformation modes, Journal of Sound and Vibration 198 (5) (1996) 617–637.
[11] M.A. Brown, A.A. Shabana, Application of multibody methodology to rotating shaft problems, Journal of Sound and Vibration 204 (3) (1997) 439–457.
[12] K. Hu, Z.P. Mourelatos, N. Vlahopoulos, Afinite element formulation for coupling rigid and flexible body dynamics of rotating beams, Journal of Sound and Vibration 253 (3) (2002) 603–630.
[13] W. Chuang, Analysis of the Crankshaft/Main-Bearings System of a Multi-Cylinder Engine, Ph.D. Dissertation, The University of Michigan, Ann Arbor, 1991.
[14] J.F. Booker, Dynamically loaded journal bearings: mobility method of solution, Transactions of the American Society of Mechanical Engineers, Journal of Basic Engineering, Series D 87 (1965) 537–546.
[15] J.F. Booker, Dynamically loaded journal bearings: numerical application of the mobility method, Transactions of the American Society of Mechanical Engineers, Journal of Lubrication Technology 93 (1) (1971).
[16] Z.P. Mourelatos, An efficient crankshaft dynamic analysis using substructuring with Ritz vectors, Journal of Sound and Vibration 238 (3) (2000) 495–527.
[17] H. Katano, A. Iwamoto, T. Saitoh, Dynamic behavior analysis of internal combustion engine crankshafts under operating conditions, Institute of Mechanical Engineering, Paper No. C430/049, 1991, pp. 205–216.
[18] L.S. Mayer, J. Zeischka, M. Scherens, F. Maessen, Analysis of flexible rotating crankshaft with flexible engine block using MSC/NASTRAN, DADS, MSC World Users' Conference, 1995.
[19] I.T. Martin, B. Law, Prediction of crankshaft and flywheel dynamics, Institute of Mechanical Engineering, Paper No. C382/046, 1989.
[20] B. Law, A.K. Haddock, Prediction of main bearing and crankshaft loading in reciprocationg engines, 15th CIMAC Congress, Paris, 1983.
[21] H. Okamura, A. Shinno, T. Yamanaka, A. Suzuki, K. Sogabe, A dynamic stiffness matrix approach to the analysis of three-dimensional vibrations of automobile engine crankshafts: part 1—background and application to free vibrations, ASME Winter Annual Meeting, Dallas, TX, 1990.

[22] T. Morita, H. Okamura, A dynamic stiffness matrix approach to the analysis of three-dimensional vibrations of automobile engine crankshafts: part 2—application to firing conditions, ASME Winter Annual Meeting, Dallas, TX, 1990.
[23] H. Okamura, T. Morita, Influence of crankshaft-pulley dimensions on crankshaft vibrations and engine-structure noise and vibrations, Proceedings of the SAE International Noise and Vibration Conference, Traverse City, MI, SAE Paper No. 931303, 1993, pp. 329–338.
[24] D.J. Nefske, S.H. Sung, Coupled vibration response of the engine crank-block system, American Society of Mechanical Engineers Publication DE 18-4 (1989) 379–385.
[25] Z.P. Mourelatos, A crankshaft system model for structural dynamic analysis of internal combustion engines, Computers and Structures CAS2771 (2001) 1–19.
[26] Z.P. Mourelatos, An efficient journal bearing lubrication analysis for engine crankshafts, Tribology Transactions 44 (3) (2001) 351–358.
[27] A.A. Shabana, Dynamics of Multibody System, 2nd Edition, Cambridge University Press, Cambridge, 1998.
[28] R.R. Craig Jr., M.C.C. Bampton, Coupling of substructures for dynamic analysis, American Institute of Aeronautics and Astronautics Journal 6 (7) (1968) 1313–1319.
[29] S.H. Lee (Ed.), MSC/NASTRAN, Version 67, Handbook for Nonlinear Analysis, The Macneal–Schwendler Corporation, 1992.
[30] K.J. Bathe, Finite Element Procedures, Prentice-Hall, Inc., Englewood Cliffs, NJ, 1996.